

Application of 3D X-ray CT scanning techniques to evaluate fracture damage zone in anisotropic granitic rock

M.H.B. Nasser & R.P. Young

Department of Civil Engineering, University of Toronto, Toronto, Canada

F. Rezanezhad

Cold Regions Research Centre, Wilfrid Laurier University, Waterloo, Canada

S.H. Cho,

Department of Mineral Resources & Energy Engineering, Chonbuk National University, south Korea

ABSTRACT: Barre granite's samples have been tested for fracture toughness under mode I along two different directions with respect to microstructural fabrics were investigated. 3D objects counter algorithm technique is applied on micro CT images to identify physical properties such as crack induced porosity, crack density, generated total surface area and contribution of individual mineral grains within the damaged zone. The result obtained justifies very well the fracture toughness anisotropy in Barre granite, and explains the difference in the structure of the damage zone evolving as a result of test crack interacting with pre-existing microstructural fabrics. The present study has potential application in the fields of rock mass stability, oil reservoir stimulation, rock fragmentation and damage in blasting and emplacement of dykes.

1 INTRODUCTION

Application of linear elastic fracture mechanics to understand the stress and strain at the vicinity of a crack tip continues to be a very active and challenging field of research (Irwin 1948, Barenblatt 1962, Hoagland et al., 1973). They all postulated that a "process zone" is generated in the vicinity of a propagating macrocrack tip and the notions of critical stress intensity factor, K_{IC} or effective fracture energy are a corner stone of fracture mechanics. The damage zone which is the final form of fracture process zone (FPZ) is used to describe the accumulated deformation surrounding the main crack as a whole. (Chester and Logan, 1986). The geometry of the process zone of a tensile crack was first calculated by Evans et al. (1977). The width of FPZ is considered a material property and it was found to increase with increasing grain size (Ouchterloney, 1980).

In realistic 2D and 3D tensile crack propagation processes in a polycrystalline media such as granite characterized by preferably oriented pre-existing microstructural fabric, the tensile test crack chooses its path around obstacles such as elongated quartz, feldspar or biotite grains. No attempt has been made so far to investigate the effect of preferably oriented pre-existing microstructural fabrics on the surface area of fracture path and the dimension/structure of damaged zone formed under mode I in granite.

In this study we used 3-D X-ray micro-focus CT scanning techniques to correlate between the physical properties in a damaged zone such as test cracks passage area, crack porosity (cracked volume/total volume), crack density (number of cracks per mm^3), and contribution of individual mineral grains for two different paths, perpendicular (case 1 scenario) and parallel (case 2 scenario) to pre-existing preferably oriented microstructural fabric and its correlation with measured respective fracture toughness in Barre granite. An attempt is made to relate the structural differences observed within the damage zones for these two cases to the nature of interaction between the test crack and the pre-existing microstructural fabric's orientation.

2 EXPERIMENTAL PROCEDURE AND RESULTS

2.1 Petrofabric characterization and fracture toughness measurements in Barre granite

A quantitative analysis of grain size distribution, grain aspect ratio and microcracks of Barre granite along three orthogonal directions was carried out (Nasseri et al., 2005). It is found that Barre granite is a medium to fine-grained granodiorite characterized by a very consistent composition that consists of 56% feldspar, 27% quartz, 9% biotite mica, and 6% muscovite mica and other accessory minerals. Its mineral grain size ranges from 0.25 to 3 mm. The samples used in this study are characterized by having quartz grains with an average size of 0.94 mm. The average feldspar grain size is 0.95 mm, and the corresponding average biotite grain size is 0.43 mm.

The microcracks are of intragranular to intergranular type and are found in both quartz feldspar grains and along cleavage planes of biotite grains. The grain size distribution and relevant grain shape ratio measured along two orthogonal planes are discussed in this work. The mineral grain shape has a ratio of 1.26 and 1.25 along XY (rift plane), and YZ (hard way plane) planes respectively (Nasseri and Mohanty, 2008). As is evident from the 3D block diagram of microcrack orientation in Figure 1, microcrack orientation in Barre granite are preferably oriented within the rift plane (XY, plane of easiest splitting), traces of which are clearly shown as microcracks parallel to Y-axis on YZ and to X-axes on XZ planes.

In the present study we use the cracked chevron notched Brazilian disc (CCNBD) test method (ISRM, 1995) to study the anisotropy in fracture toughness (highest K_{IC} /lowest K_{IC}) in Barre granite (Nasseri and Mohanty, 2008). The Brazilian disc samples (Figure 1) were prepared from three orthogonal planes representing the high, intermediate and low P-wave velocity directions. In this study we report only the petrofabric analysis and fracture toughness measurements related to highest and lowest planes.

Figure 2 shows the result for the fracture toughness measured along specific planes for Barre. Four to five specimens for each plane were tested in order to verify the reproducibility of K_{IC} measurements as a function of petrofabric orientation. ISRM suggested method (1995) and Iqbal and Mohanty (2006) have been adopted to perform and calculate the fracture toughness values in this paper. Barre granite specimens analyzed in this study show a fracture toughness anisotropy ratio (highest K_{IC} /lowest K_{IC}) of 1.64. The average fracture toughness for the plane representing the toughest plane in which the test crack is forced to propagate perpendicular to oriented microstructural fabric reported in this yields K_{IC} values of 1.89 ($\text{MPa}\cdot\text{m}^{0.5}$) for case 1 and the average reported in this study yields K_{IC} values of 1.89 ($\text{MPa}\cdot\text{m}^{0.5}$) for case 1 and the average fracture toughness representing the weakest plane in which the test crack is forced to propagate parallel to oriented microstructural fabric shows a K_{IC} values of 1.15 ($\text{MPa}\cdot\text{m}^{0.5}$) for case 2 scenario.

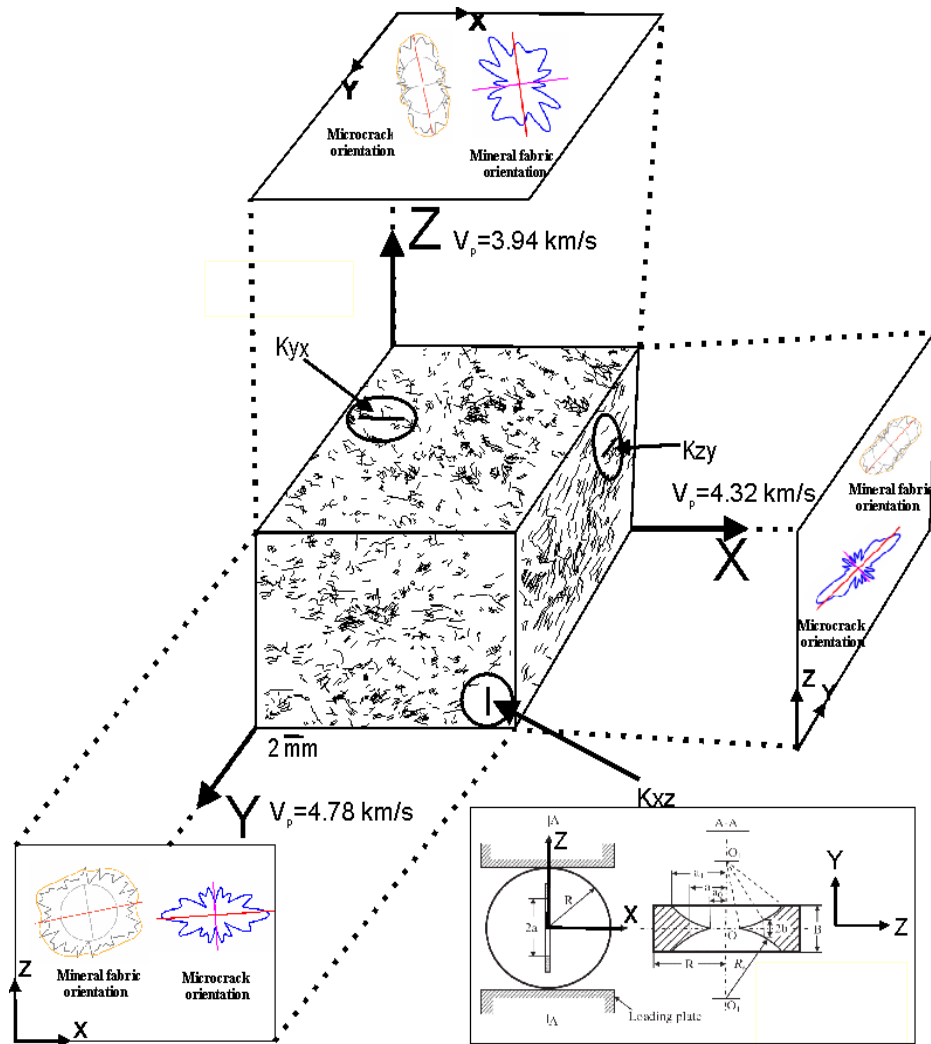


Figure 1. 3D block diagram showing microcracks orientations in Barre granite; rose diagrams show the alignment of microcracks and mineral fabric orientation for each plane. The box on the right side of the figure shows the plan and section view and the geometry of the tested specimens.

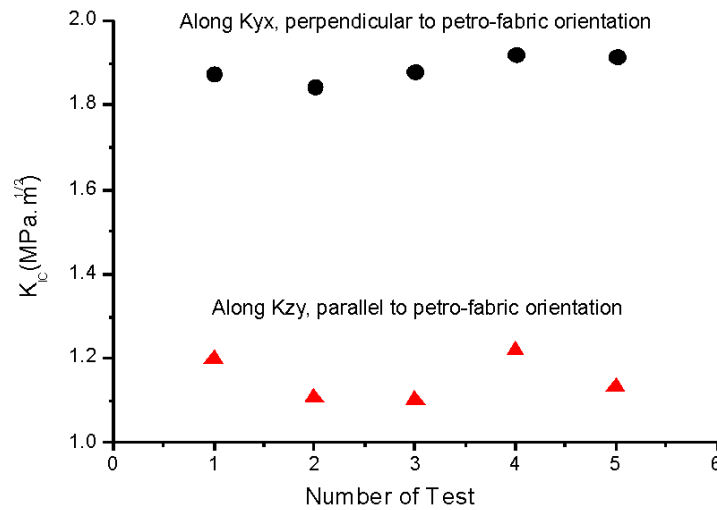


Figure 2. Variation of fracture toughness measured along perpendicular and parallel directions with respect to preferably oriented pre-existing microstructural fabric in Barre granite

2.2 Sample preparation of tested specimens for X-ray micro CT scanning

The CCNBD specimens representing the highest and the lowest fracture toughness values that had still remained intact after testing have been used for sample preparation which would be suitable for X-ray micro CT scanning. In order to minimize subsequent damages to the tested disc samples, they were impregnated with a polymer glue keeping the two halves together prior to cutting into smaller size. Figure 3 shows the stages of sample preparation procedure involving the cracked section of the specimen. This practice insures a higher resolution micro CT image.

2.3 3D X-Ray CT scanning methodology

Two samples, one containing the test crack forced to propagate parallel and the other propagate perpendicular to preferably oriented pre-existing microstructural fabric have been prepared as described above. These samples with the dimensions $10 \times 15 \times 15$ mm were carried out at the University of Hokkaido, Japan for X-ray CT scanning. It used a Toshiba Micro CT, TO-SCANNER 30900 μ hd at 90 kV with pre-filtering X-ray beam by passing it through 0.6 mm of aluminium to reduce hardening artifacts and enhance sample phases.

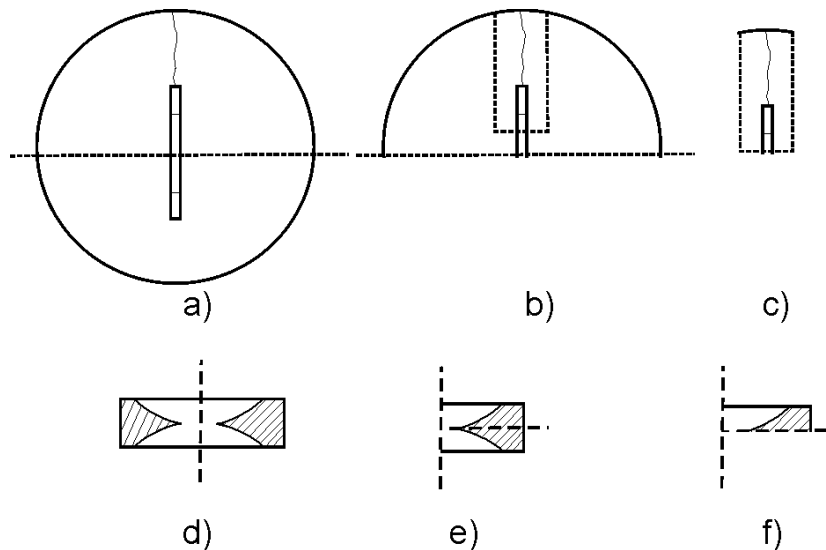


Figure 3. Various stages of sample cutting steps to prepare the smaller cracked specimen for imaging in micro CT scanning equipment. Stages a) - c) show the cutting technique on the plan view of the CCNBD specimen and stages d) - f) show the same for section view of the tested specimens.

The detector was a high resolution digital X-ray camera detector system. This detector accumulates all the energy of the transmitted photons and provides the numerical data to be used in reconstructing an image. For each head, 1500 views of the sub-sample were taken over 360° rotation. Each sample was placed vertically within the scanner so that the X-ray intersected the sample perpendicular to its longitudinal axis. Once the scans were finished the collected raw data (the series of rotational X-ray images) were reconstructed with an ultra-high resolution noise-reducing filtered back-projection algorithm (Lewitt, 1983) to derive images with good contrast between the two phases – smaller cracks associated with the test crack and the rock materials. Application of 3D X-ray CT scan has been quite helpful to understand the mechanics of failure in rocks (Kawakata, et al. 1999, Reynaud, et al. 2007). The resulting 3D imagery was acquired at size of $504 \times 960 \times 1118$ and $548 \times 997 \times 908$ voxels for the two situations where the test crack were forced parallel and perpendicular to pre-existing micro fabrics, respectively in a local 3D (XYZ) coordinate system with a resolution of $0.007 \times 0.007 \times 0.007$ mm for each voxel. An example of 3D CT images rendering of the test and smaller-crack spaces are shown in Figure 4.

2.4 Damage zone assessment

The spatial resolution of the CT scans was sufficiently high, and hence the high attenuation contrast between voids (induced cracks, test crack and associated ones) and solid material (mineral grains) allows direct imaging of individual cracks and its networks. In general, induced cracks were characterized by low densities, and mineral grains were characterized by high densities. Using 3D digital image analysis techniques, the induced crack distribution within tested samples was quantified. The surface area and volume of induced cracks were measured by a “3D Objects Counter” algorithm in *ImageJ*. This algorithm provides an accurate segmentation into binary images that allows for the frequency (i.e. number of individual cracks) measurements as well as some morphology characteristics (individual crack volume and surface area, the centre of mass and the centre of intensity) for each separable crack.

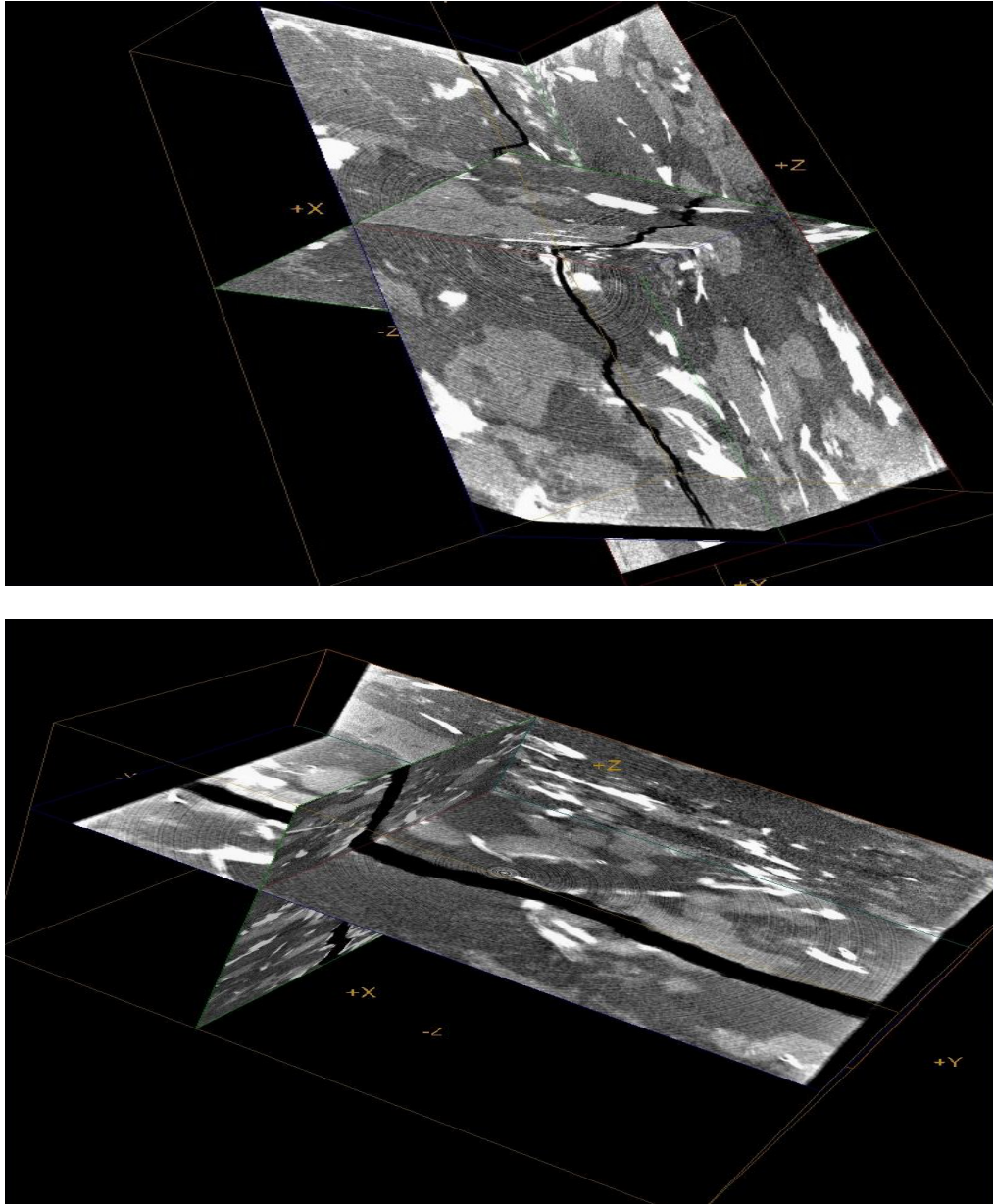


Figure 4. 3-D micro CT image on the top shows the propagation of the test crack perpendicular to pre-existing micro-fabric orientation and the 3-D image on the bottom shows propagation of test crack parallel to micro-fabric orientation.

We employed the 3D Objects Counter algorithm on 3D CT images of Barre granite samples to identify the physical properties such as crack porosity (crack volume/total volume) and density (i.e. number of cracks per mm³) and newly generated total crack surface area. The summary results including the comparisons between the fracture toughness obtained for case 1 and 2 scenarios and that of morphometric analysis obtained from three-dimensional CT scanning images are presented in Table 1. The crack porosity (ϕ_f) was computed as the total volume of empty smaller cracks divided by the total volume of the image from sample (V_{img});

$$\phi_f = \sum V_i / V_{img}, \quad [1]$$

where V_i [L³] is the volume of the i -th smaller crack on all total volume voxels.

Table1: Summary of 3-D analysis of micro CT images obtained from the test crack and the damage zones (smaller cracks) for both cases. Measured fracture toughness for both cases is included.

Propagation With Respect to Micro-fabric Orientation	Induced crack porosity, in damage zone only %	Number of cracks, in damage zone only	Volumetric crack density, in damage zone only crack/mm ³	Total crack passage area test crack & damage zone (mm ²)	K _{IC} MPa m ^{0.5}
Case1-Perpendicular	0.014	223	1.31	28.32	1.9
Case 2-Parallel	0.001	24	0.14	14.65	1.1

2.5 Image analysis and separation of test cracks, associated cracks in damage zone and mineral constituents

The analysis of the processed images was carried out by using open source software GE-HC Microview v2.1.1 (<http://sourceforge.net/projects/microview>) and ImageJ 1.40g (<http://rsbweb.nih.gov/ij/>). The fraction of the voids filled with air (cracks or damaged volume/total volume) can be calculated from the CT image of the granite samples using image segmentation techniques where the ratio between the volume of empty space and the total volume of the sample can be calculated. This step is crucial and can lead to inaccuracies because of the nature of the CT image and the sensitivity of image segmentation techniques. It can reduce or increase the estimate of void space and blur or make an apparent connection between them. In order to achieve an accurate separation of voids (induced cracks) from the solid matrix (minerals), a new neighbourhood-based standard deviation thresholding algorithm (Elliot and Heck, 2007) was applied for CT images. This method is based on the range of X-ray linear attenuation coefficient that was expressed in a dimensionless quantity known as Hounsfield Units (HU). It relates to the density of materials with an intensity value between -1000 and 1000. The large density difference between void (HU = -1000), and the remaining constituents of mineral grains (HU = ~400-1000) represented by the non-void voxels, allows direct imaging of individual induced cracks and their networks. This procedure is a quantitative approach to select a threshold that involves fitting a Gaussian distribution to a bi-modal distribution on a histogram of relative density. In this method the user selects the threshold that appears to best separate the grey level classes associated with minerals and voids (cracks). In this technique, the original grey-level microtomographic images were processed using ImageJ to produce a binary images after segmentation of the crack voids and solid phases, in which void phase voxels are black and solid phase voxels are white. This approach helps to calculate the crack passage area within the three distinguishable main constituent or minerals in micro CT images obtained from Barre granite for case 1 and case 2 scenarios. Table 2 summarizes the above said statistical evaluation.

Furthermore the test crack passage area and the associated ones within the damage zone of case 1 scenario contributes about 26.86 mm² and 1.45 mm² of the total crack passage area. The test crack and associated ones for case 2 scenario measure to 14.5 mm² and 0.11 mm² of the total crack passage area for same volume of rocks.

In terms of contribution of various minerals to total crack passage area, for case 1 scenario, feldspar, quartz and biotite accommodate 12.86, 7.06 and 4.17 mm² of total crack passage area of 24.1 mm² respectively. Whereas for case 2 this proportion is 6.51, 4.82 and 1.94 mm² for a total crack passage area of 13.27 mm². The total percentage obtained from the individual contribution of three types of minerals towards the total passage cracked area in both cases does not add up to make 100%. This can be due to lack of proper identification of grey colour spectrum by the software or can also be contributed to the situations in which the test crack travelled along the grain-grain boundaries in two scenarios. This discrepancy will be further verified in future analysis. As shown in Figure 3 these analysis includes only ¼ of the total area of surfaces generated. The analysis of the percentage of passage area within individual mineral type, contributing towards their respective total crack passage area in both cases matches well with the Barre granite's global percentage of mineral composition (Table 2). On the other hand the total crack passage area in case 1 (28.32 mm²) for a given volume of tested specimen is twice of what has been measured for case 2's total crack passage area (14.65 mm²) for similar volume of specimen studied. Assuming symmetrical generation of cracked surface area for both notches in case 1 and 2, one can calculate the total generated crack passage area to be approximately about 113.28 mm² and 58.6 mm² respectively for these cases.

Table 2: Contribution of individual minerals towards total passage area of test crack obtained from X-ray micro CT image analysis and its correlation with fracture toughness for case 1 and 2 scenarios.

Test crack	Crack passage area in biotite (White) mm ²	Crack passage area in quartz (Light Gray) mm ²	Crack passage area in feldspar (Dark Gray) mm ²	Total crack passage area mm ²	K _{IC} MPa.m ^{0.5}
Case-1 Perpendicular	4.17	7.06	12.86	24.10	1.9
%	15.55	26.3	47.9	~90	
Case-2 Parallel	1.941	4.82	6.51	13.27	1.1
%	13.35	33.17	44.83	~91.5	

2.6 Comparison of the structure of the process/damage zones for two scenarios

Visual analysis (Figure 5) of the test crack morphology along successive vertical and horizontal planes for case 1 scenario shows that the test crack is characterized with more branching in the upper section (within the rectangular section of the notch) where propagation is believed to occur in an unstable manner (Nasseri et al., 2006).

Generally this test crack is characterized with numerous deflections, branching and terminations specially encountering elongated minerals with their longer axis oriented at higher angle with respect to propagation direction. The width of the damage zone becomes larger and is characterized with numerous longer subsidiary branches. It is observed that the subsidiary branches follow the grain-grain boundaries between quartz and feldspars and they also tend to rejoin with the main crack. On the contrary the test crack for case 2 scenario does not show any major deflection and lacks subsidiary branching and its damage zone is confined to a smoother plane and narrower volume within the width of the test crack itself (Figure 5, bottom series).

3 DISCUSSION

3.1 *Factors affecting fracture propagation*

One of the disciplines where the research on the fracture process zone mechanism/size has taken a lead is the ceramic industry. The relationship between the toughening mechanism and microcracking has been studied experimentally and theoretically (Evans, 1990). Although progress in this field has been appreciable, there is incomplete understanding of the degradation caused by the microcracks directly ahead of the crack front and limited knowledge of the interaction between modulus and dilatational contribution to crack shielding/amplification (Hori and Nemat Nasser, 1987, Chen, 2003) as well as experimental microcrack detectability limitations. In situation where the initial orientation of micro fractures or weakness planes ahead of the test crack may be different due to the random orientation of crystals, the micro fractures will align themselves with preferred cleavage planes and that may not be parallel to the plane of the test crack propagation direction causing local deviation.

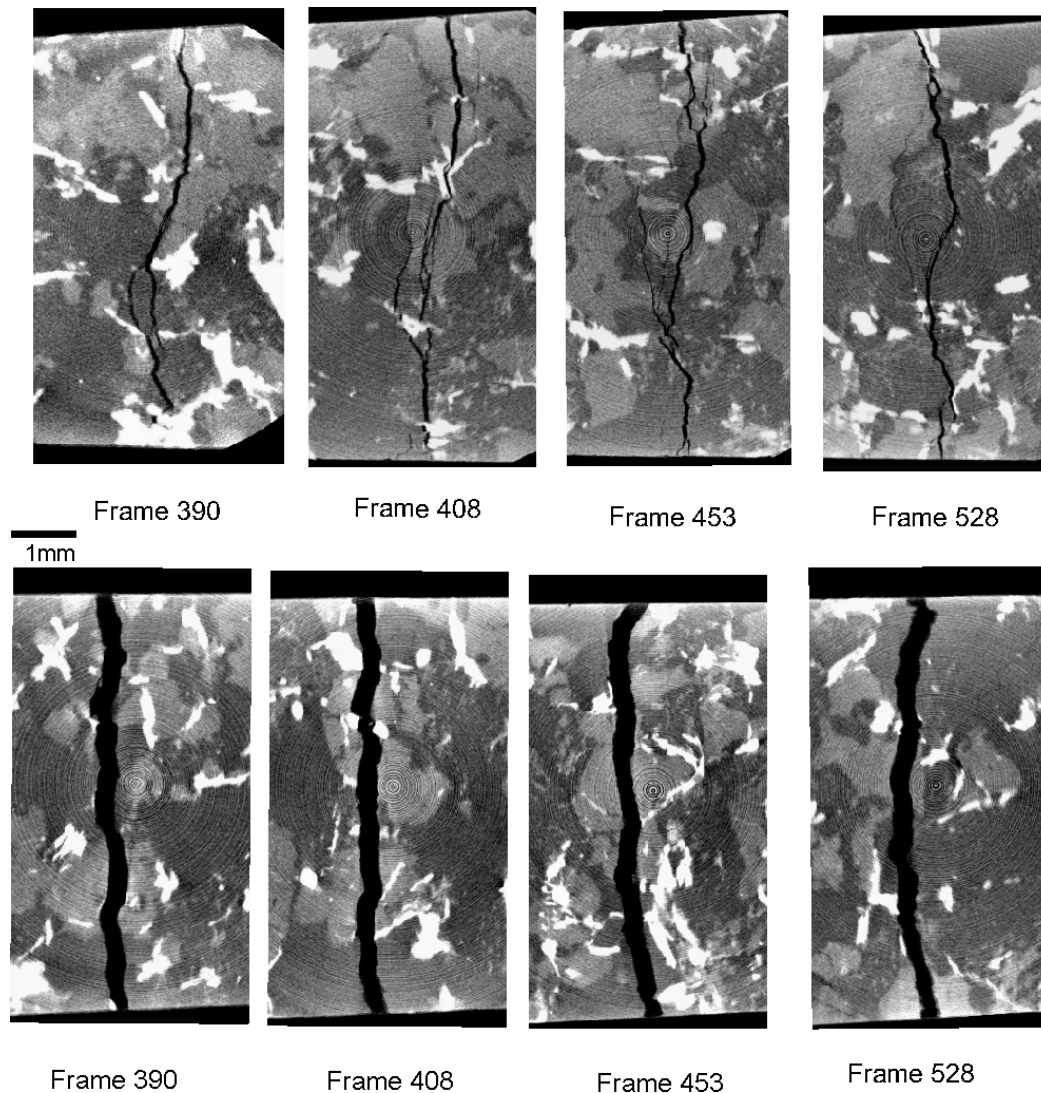


Figure 5. X-ray micro CT images showing the comparison between the structure and width of the damage zone for case 1 (top series) and case 2 (bottom series) along horizontal plane (XY). Note that in top series the test crack is deflected, branched and the damage zone is wider in comparison to the test crack's structure and damage zone width in the lower series (case 2). The width of the test-crack in the lower series is not to the scale and is due to sample preparation artifact.

It has been observed that simultaneous propagation of series of microcracks and their interacting with test crack ahead at its tip causes enhanced energy dissipation. This idea is supported by a series of experiments performed by Ravi-Chandra and Kaunass, (1984) on the brittle Homalite 100. Observation of series of test crack profile in present study along vertical and horizontal planes for case 2 shows that the associated cracks are confined within a narrow damaged zone running almost parallel with the main crack and does not show much branching of the main crack (Figure 6).

Lower number of subsidiary cracks; smaller length and smaller and smoother crack passage area (Table 1 & 2) within studied volume suggest a mechanism in which the test crack propagates via connecting pre-existing favorably oriented microstructure for case 2 scenario. Nasseri et al., (2007), have concluded that there exist a positive correlation between the fracture toughness and fracture roughness as a function of microstructural fabric orientation in Barre granite. In situations where the distance from the crack tip to the nearest high density microstructural element being negligible, lead to minimum crack path deviation and resistance. In literature micro branching in brittle materials is related to fracture growth instability during dynamic propagation in brittle material (Sagy et al., 2001). And it has been shown that as unstably loaded fracture reaches its limiting propagation velocity; the crack bifurcates, adding additional surface area in order to dissipate further energy and limit propagation velocity, (Kanninen and Popelar, 1985; Marder and Fineberg, 1996).

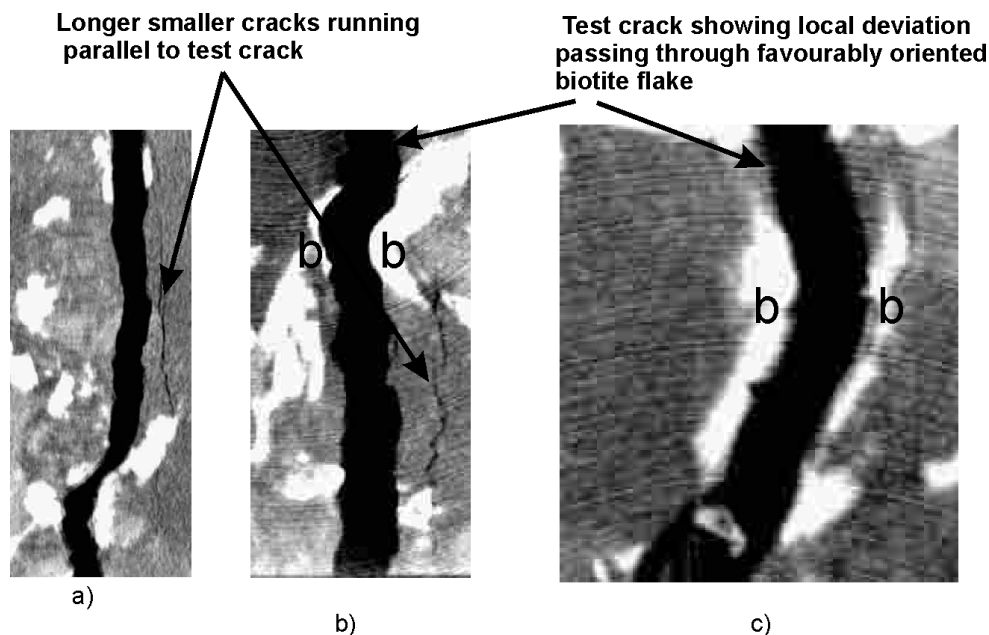


Figure 6. a) & b) Showing smaller associated crack in the damage zone for case 2 scenario along XZ (vertical) and XY (horizontal) planes respectively, c) Deviation of test crack along cleavage plane of favorably oriented biotite grain in case 2 scenario. Biotite minerals are shown as b in this figure.

Though the fracture velocity variation/comparison is not being studied in this paper, it is believed that in both cases the nature of interaction between the test crack and microstructural fabric triggers branching of different types. In this study the phenomena of the test crack branching is quite pronounced in case 1 in which the longer subsidiary branches have a rough profile and most of them initiate around places involving favorably oriented biotite flakes, encouraging test crack branching due to cleavage plane splitting (Figure 7a & 7).

Micro CT image analysis and observation in Case 1, show intersection of test crack with unfavorably oriented (at right angle) sets of biotite flakes at different distances along its vertical and horizontal planes (Fig. 7 a & b). Another factor is the angle of incidence between the test

crack and orientation of cleavage plane in biotite which affects its branching/deflection and termination. This resembles a similar situation where toughening mechanisms is enhanced in ceramic industry using fiber-reinforced matrix composites as shown in figure 7c. It is shown that in fiber reinforced ceramics which fracture by the growth of a single dominant flaw in Mode I, phenomena such as debonding, frictional dissipation, residual stresses and stored elastic energy relationship between the matrix and the fiber contribute positively towards toughness (Evans, 1990). This is a good analogy for case 1 scenario which records a higher fracture toughness and much more surface area generation than case 2.

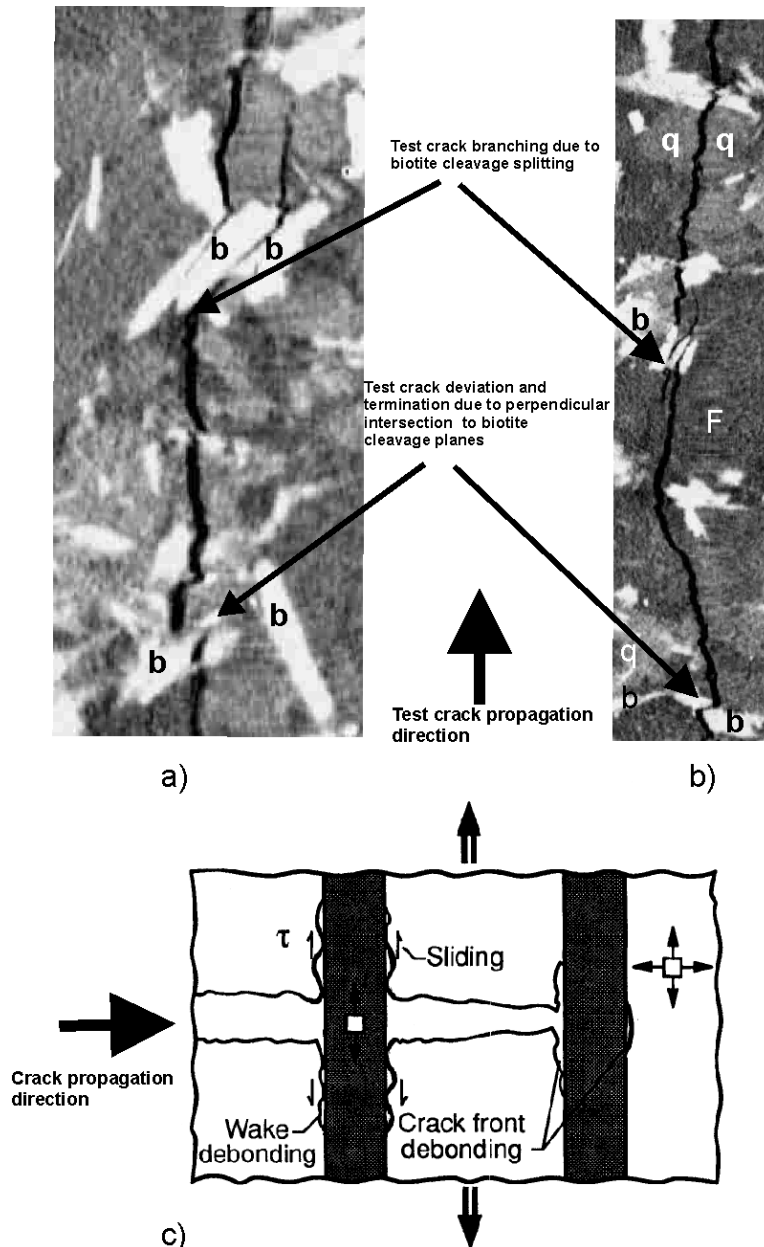


Figure 7 a) & b) CT images taken from the vertical section of the test crack in case 1 scenario showing different types of test crack interaction with preferably oriented biotite minerals, b, q and F stand for biotite, quartz and feldspar grains, c) Schematic illustration of the debonding of fibers that are oriented at right angle to the crack front propagation and sliding in the crack wake (Evans, 1990).

4 CONCLUSIONS

3D micro CT images are used to understand the relationship between the test crack path propagation/damage zone and nature of its structure and the microstructural fabric orientation in Barre granites. The damage zone for the situation in which the test crack is forced to propagate perpendicular (case 1) to pre-existing microstructural fabrics is characterized with almost twice newly generated crack surface area. The measured induced crack porosity for the same case is more than ten times that of when the crack is forced to propagate parallel to the orientation of pre-existing microstructural fabrics (Case 2). This conclusion further justifies the reason for the fracture toughness in case 1 being almost twice of that of case 2.

It is also concluded that the nature of interaction between the test crack and pre-existing microstructural fabric's orientation dictates the type and structure of the branched and the subsidiary parallel cracks in the damage zone in case 1 and 2 respectively. As a result of such an interaction many long branches originate from the main crack, making the damage zone more complex and wider in size in case 1 scenario. Whereas, the damage zone in case 2 scenario is characterized with subsidiary cracks that run more or less parallel to the main crack and are shorter in length.

These observations may be applied to the field scale of various size in which the stress induced tensile forces promote fracture propagating quasi-statically. Rift zones, sites for dyke intrusion and supporting roof of a mine under tension are good examples. Depending on the nature of interaction of propagating tensile fractures with pre-existing oriented sets of geological structures, a rougher crack profile and more damaged rock masses can be formed. This will eventually affect the post strength, post-frictional and hydro-geological and flow regime properties of resultant rock mass. The present study, linked with observations in field scale will help in better understanding of fracture propagation/interaction and its application to enhance the natural stability of underground openings, control of rock fragmentation and damage in blasting, prediction of transport properties with diverse flow regimes in rocks and enhancement of oil reservoirs during hydraulic fracturing.

Acknowledgment: The authors would like to thank Professor Kaneko at Hokkaido University in Japan for help in acquisition of the X-ray CT scanned images. Discussion with Professor Mohanty and his comments on the manuscript are greatly appreciated.

5 REFERENCES

- Barenblatte, G.I. 1962. The mathematical theory of equilibrium cracks in brittle fracture. *Advances of Applications Mechanics* 7:55-129.
- Chester, F.M. & Logan, J.M. 1986. Implications for mechanical properties of brittle faults from observations of the Punchbowl fault zone, California. *Pure Applied Geophysics* 124:79-106.
- Chen, C.K. 2003. Near-tip microcrack shielding in advanced ceramics. *Fatigue Fract Engng Struct* 27: 45-50.
- Elliot, T.R. & Heck R.J. 2007. A comparison between 2D vs 3D thresholding of X-ray CT imagery. *Canadian Journal of Soil Science* 84(4): 405-412.
- Evans, A.G., Heuer, A.H. & Potter D.L. 1977. The fracture toughness of ceramics. *Fracture* vol. I ICF4 529-556, Waterloo, Ontario, Canada.
- Evans, A.G. 1990. Perspective on the development of high-toughness ceramics. *Journal of American Ceramics Society* 73(2): 187-206.
- Hoagland, R.G. Hahn, G.T. & Rosenfield, A.R. 197. Influence of microstructure on fracture propagation in rock. *Rock Mechanics* 5:77-106.
- Hori, M. & Nemat-Nasser, S. 1987. Interacting micro-cracks near the tip in the process zone of a macro-crack. *J Mech Phys solids* 35:601-629.
- Irwin, G.R. 1948. Fracture dynamics. *Fracture of Metals, American Society Metal Transaction Quarterly*, Cleveland 40A:147-166.
- ISRM (1995). Suggested method for determining Mode I fracture toughness using cracked chevron notched Brazilian disc (CCNBD) specimens. *Int. J Rock Mech. Min Sci. Geomech Abstr.* 32:57-64.

- Kanninen, M.F. & Popelar, C.H. 1985. *Advanced Fracture Mechanics*. Oxford Univ. Press, New York.
- Kawakata, H. Cho, A. Kiyama, t. Yanagidani, T. Kusunose, K. & shimada, M. 1999. Three-dimensional observations of faulting process in Westerly granite under uniaxial and triaxial conditions by X-ray CT scan. *Tectonophysics* 313: 293-305.
- Lewitt, R.M. 1983. Reconstruction algorithms: Transform methods. *Proc. IEEE* 71: 390-408.
- Iqbal, N., & Mohanty, B. 2006, Experimental calibration of stress intensity factors of the ISRM suggested cracked chevron-notched Brazilian disc specimen used for determination of mode-I fracture toughness: *Int J Rock Mech Min Sci* 43:1270-1276.
- Marder, M. & Fineberg. 1996. How things break. *Physics Today* 49:24-29.
- Nasseri, M.H.B. Mohanty, B. Robin, P-YF. 2005. Characterization of microstructures and fracture toughness in five granitic rocks. *Int J Rroc Mech Min Sci* 42: 450-60.
- Nasseri, M.H.B. Mohanty, B. & Young, P.R. 2006. Fracture toughness measurements and acoustic emission activity in brittle rocks. *Pure Applied Geophys.* 163:917-945.
- Nasseri H.H.B. Grasselli, B. Mohanty, B. Wirth, j. & Braun, M. 2007. Experimental relationship between fracture toughness and fracture roughness in anisotropic granitic rocks. VOL 1. 617-624. Proc. 1st Canada-US rock mechanics symposium Vancouver, Canada 27-31 May. Taylor & Francis.
- Nasseri, M.H.B. Mohanty, B. 2008. Fracture toughness anisotropy in granitic rocks. *Int J Rock Mech Min Sci* 45: 167-193.
- Ouchterlony, F. 1980. Review of fracture toughness testing of rocks. DS 15, Swed. Detonic Res, Found., Stockholm.
- Raynaud, S. Naga-tillard, D. Desrues, J.& Mazerolle, F. 2007. Brittle-to-ductile transition in Beaucaire marl from triaxial tests under the CT-scanner. *Int J Rock Mech Min Sci* 45: 653-671.
- Ravi-Chandar, K. & Knauss, W.G. 1984a. An experimental investigation into dynamic fracture: I. Crack initiation and arrest. *International Journal of Fracture* 25:247-262.
- Segy, A.S. Reches, E. & roman, I. 2001. Dynamic fracturing: Field and experimental observations. *Journal of Structural Geology* 23 (8): 1223-1239.